

# We are IntechOpen, the world's leading publisher of Open Access books Built by scientists, for scientists

6,900

Open access books available

186,000

International authors and editors

200M

Downloads

Our authors are among the

154

Countries delivered to

TOP 1%

most cited scientists

12.2%

Contributors from top 500 universities



WEB OF SCIENCE™

Selection of our books indexed in the Book Citation Index  
in Web of Science™ Core Collection (BKCI)

Interested in publishing with us?  
Contact [book.department@intechopen.com](mailto:book.department@intechopen.com)

Numbers displayed above are based on latest data collected.  
For more information visit [www.intechopen.com](http://www.intechopen.com)



# ZnO Nanorods for Gas Sensors

*Yanmin Wang*

## Abstract

ZnO nanorods have been widely used to detect low-concentration gases due to its range of conductance variability, response toward both oxidative and reductive gases, and highly sensitive and selective properties. In this chapter, the fabrication methods of ZnO nanorods, their controllable growth, their different configurations, their modification for improving sensing property, and their composites for gas sensors are thoroughly introduced. The synthesis methods to fabricate ZnO nanorods consist of hydrothermal method, microemulsion synthesis, microwave-assisted hydrolysis preparation, gas-solution-solid method, spray pyrolysis, sonochemical route, simple solution route, and so on. The controllable fabrication of ZnO nanorods can be realized by control growth, selective growth, and diameter regulation. Different structures formed by ZnO nanorods include cross-linked configuration, flowerlike structure, and multishelled hollow spheres and hollow microsemispheres, as influence their sensing properties. ZnO nanorods can be modified by doping, functionalization, decoration, and sensitization for enhancing the sensing property. ZnO can be combined with graphene, carbon nanotubes, SnO<sub>2</sub>, In<sub>2</sub>O<sub>3</sub>, and Fe<sub>2</sub>O<sub>3</sub> to form core-shell composites for gas sensor.

**Keywords:** ZnO nanorods, fabrication, modification, composites, gas sensor

## 1. Introduction

With the development of economy and society, the increasingly serious environmental problems have become the world topics of concern to people. Gas sensors have been widely used in medicine industry and ecology to protect people from harmful gases [1]. Generally, gas-sensing mechanism is founded on the electron transport between adsorbed oxygen species and test gas molecules [2]. The response of sensor is not only determined by the amount of adsorbed oxygen species but also by the specific surface area, structure, active sites, and electron properties of sensing materials.

Metal oxide semiconductor sensors have attracted great attention for a long time because they have advantages such as low cost, online operation, low power consumption, high sensitivity under ambient conditions, and high compatibility with microelectronic processing [3]. Metal oxide gas sensors function through controlling the electrical conductivity upon exposure to gases. A number of metal oxides, such as TiO<sub>2</sub>, ZnO, SnO<sub>2</sub>, Fe<sub>2</sub>O<sub>3</sub>, WO<sub>3</sub>, etc., have been employed for gas sensors [4].

Among them, ZnO has been widely used to detect low-concentration gases, such as ethanol, benzene, nitrogen oxide, liquid petroleum gas, and other species due to a wide band gap, low-cost environmentally benign components, nontoxicity [5], good thermal and chemical stability, high-electron mobility, large exciton binding energy, and its range of conductance variability and response toward

both oxidative and reductive gases [6, 7]. Since ZnO thin film was used to detect gaseous components at about 400°C for the first time in 1966 [8], ZnO has been widely investigated due to its good and stable gas-sensing properties. Various ZnO morphologies provide different sensing performances [9]. For instance, ZnO nanopetals have a sensitivity of 119–20 ppm NO<sub>2</sub> gas at room temperature [10]. Monodisperse ZnO hollow six-sided pyramids have a sensitivity of about 15 to dimethylformamide (DMF) and 187 to ethanol [11]. The flowerlike ZnO nanostructures showed the highest response of 144.38 and excellent selectivity to ethanol 500 ppm at 360°C [12].

Gas sensors based on one-dimensional ZnO nanostructures have recently attracted much attention due to its high sensitivity and low power consumption [13, 14]. Especially ZnO nanorods have been widely used for detecting low-concentration gases due to its range of conductance variability, response toward both oxidative and reductive gases, and highly sensitive and selective properties. In this chapter, the fabrication methods of ZnO nanorods, their controllable growth, their different configurations, their modification for improving sensing property, and their composites for gas sensors are thoroughly introduced.

## 2. Fabrication methods of ZnO nanorods

### 2.1 Hydrothermal method

A two-step low-temperature hydrothermal method was adopted to synthesize ZnO nanorods (NR) selectively grown on-chip as shown in **Figure 1**. The electrodes of Pt on Cr were fabricated by sputter deposition and lift-off technique on a glass substrate (**Figure 1(A)**). On a glass substrate, small zinc islands were sputter deposited as nucleation sites for the ZnO nanorod growth (**Figure 1(B)**). In the next two steps, an equimolar solution of Zn (NO<sub>3</sub>)<sub>2</sub>·6H<sub>2</sub>O and (CH<sub>2</sub>)<sub>6</sub>N<sub>4</sub> was used. The solution was used for growth nucleation of short ZnO nanorods in the first step (**Figure 1(C)**), whereas it was used for the nanorods elongation in the second step (**Figure 1(D)**). Nanorod junctions were formed by the connection of long porous nanorods from neighboring islands.

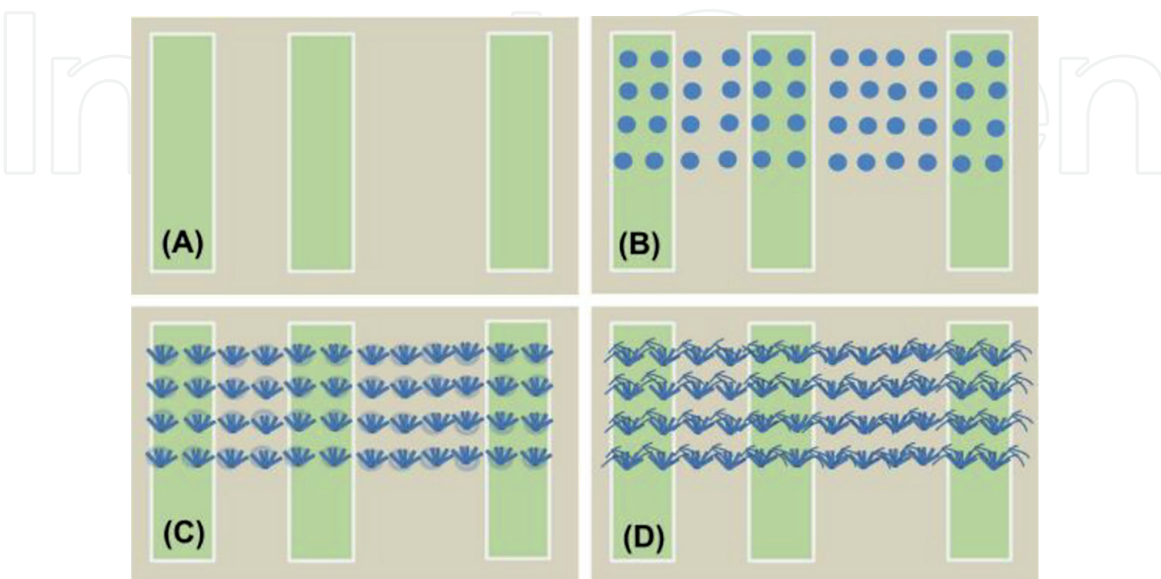


**Figure 1.** Formation of ZnO NRs junctions by two-step hydrothermal growth: (A) deposition of Pt electrodes, (B) deposition of Zn seed islands, (C) growth of dense ZnO nanorods (first step), and (D) growth of long porous ZnO nanorods (second step).

**Figure 2(A)** shows the SEM images of the sensing part of the ZnO NR sensor. As shown in **Figure 2(A)** and **(B)**, the isolated islands were designed as nucleation sites for creating NR junctions within the conducting path from one electrode to the other of the sensor. ZnO NRs in **Figure 2(C)** is a porous material formed from nanocrystals, and its surface is very rough. The measurement of the nanorod gas sensor toward NO<sub>2</sub>, ethanol, hydrogen, and ammonia indicated that the sensitivity to NO<sub>2</sub> was the highest [15].

## 2.2 Microemulsion synthesis

Zinc oxide nanorods were prepared by surfactant-assisted microemulsion method. The microemulsion for the synthesis of ZnO nanorod consists of surfactant such as ethyl benzene acid sodium salt (EBS), dodecyl benzene sulfonic acid sodium salt (DBS), and zinc acetate dihydrate (ZnAc<sub>2</sub>·2H<sub>2</sub>O) in xylene. Then the mixture solution of hydrazine monohydrate and ethanol was added drop-wisely to the microemulsion at room temperature by simultaneous agitation. After refluxing the resulting precursor-containing mixture and centrifuging the milky white suspension, the precipitate was rinsed and dried [16].

The aspect ratio of ZnO nanorods was affected by the alkyl chain length of surfactant. ZnO nanorods synthesized by EBS with short alkyl chain length show higher aspect ratio than those by DBS. The response of ZnO nanorods to CO in air was strongly affected by the surface area, defects, and oxygen vacancies. Therefore, ZnO nanorods synthesized by the microemulsion synthesis have large aspect ratio and enhanced gas-sensing properties.

## 2.3 Microwave-assisted hydrolysis preparation

Highly oriented (002) plane-bounded ZnO nanorods ended with a surface defect hexagonal plane were prepared through microwave-assisted hydrolysis and used as a CO gas detector [17]. In the growth process, growth solution was prepared by dissolving zinc nitratehexahydrate (ZnNO<sub>3</sub>·6H<sub>2</sub>O) and hexamethylenetetramine

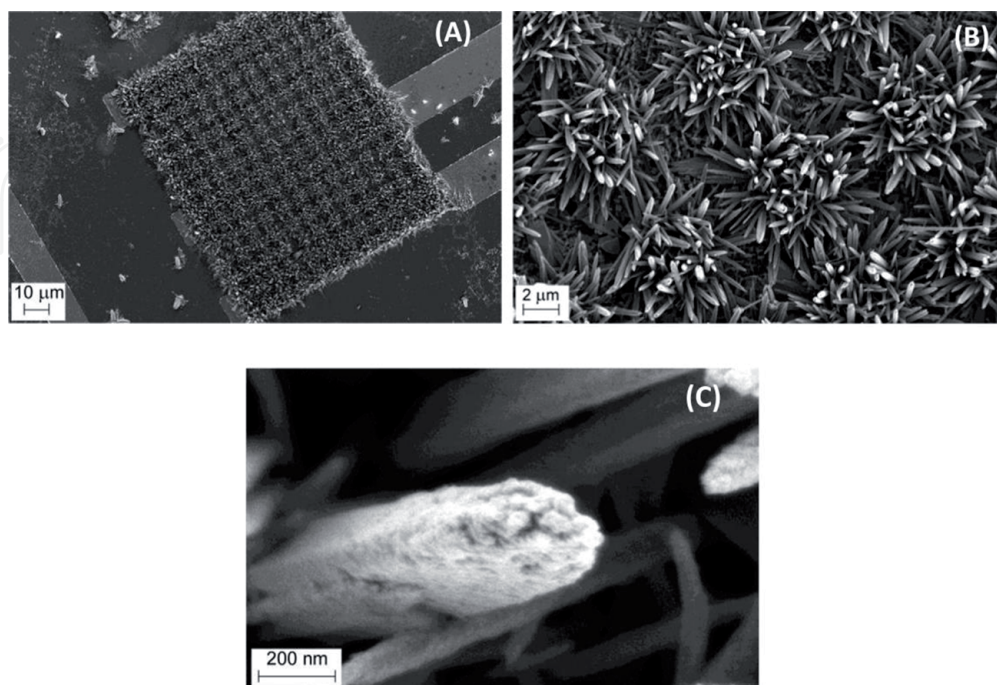


**Figure 2.**  
(A) SEM image of ZnONRs synthesized with hydrothermal method at 85°C within Pt electrodes. (B) Higher magnification of ZnO NRs grown from different islands making NR junctions. (C) Image of a single ZnO NR.

(HMT) in deionized water. Subsequently, a seeded-FTO substrate immersed in the growth solution was processed in the microwave oven. The sensor with these ZnO nanorods presented a remarkable response at 81.1% toward 100 ppm CO gas exposure and recovery time of approximately 2.5 min. The microwave-assisted hydrolysis is an excellent approach to fabricate ZnO nanorods used for low-concentration CO gas detection system at room temperature.

## 2.4 Gas-solution-solid method

ZnO nanorod arrays on Zn substrate were prepared by the so-called gas-solution-solid method [18]. The aligned ZnO nanorods on substrates were obtained by putting Zn foils above an ammonia solution. The growth mechanism is studied and proposed as shown in **Figure 3**. The Zn foil is first put above the ammonia solution (**Figure 3-1**). The evaporation and condensation of ammonia solution formed a thin layer on the surface of Zn foil (**Figure 3-2**). At the beginning of ZnO nanorod growth, Zn on the surface of substrate is oxidized by O<sub>2</sub> to produce ZnO, as then reacts with NH<sub>4</sub>·OH to form Zn(OH)<sub>2</sub> in the thin layer of ammonium solution. The putative reactions relevant to the synthesis of the aligned upright ZnO nanorods are as follows:

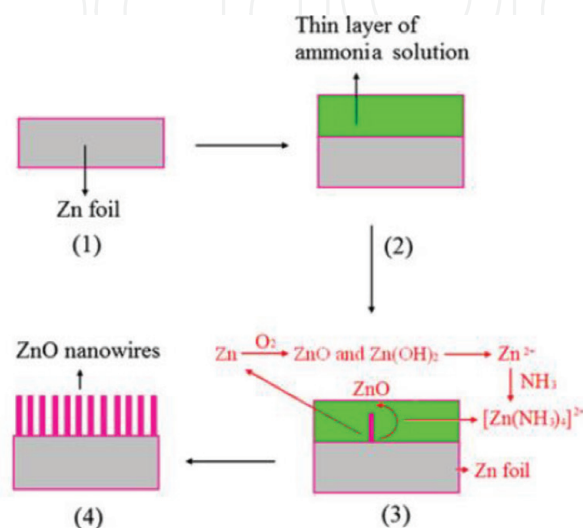
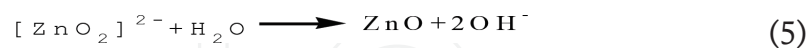
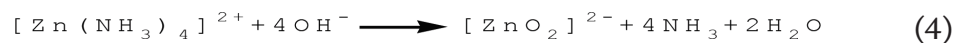
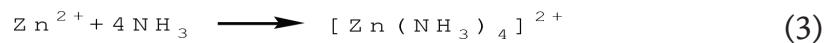
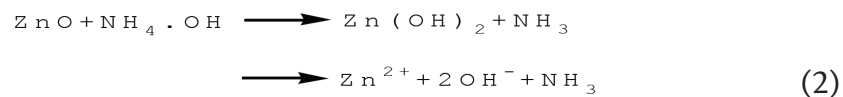


**Figure 3.** Schematic diagram showing the ZnO nanorod arrays growth.

According to the Bravais-Donnay-Harker law, once nucleate, crystal planes with smaller  $dhkl$  values grow faster, and the ZnO growth along [0001] is much faster than that along other directions. Ammonia in the solution acts as a transporter of  $Zn^{2+}$  ions (**Figure 3-3**). Finally, ZnO nanorod arrays are formed on Zn substrates (**Figure 3-4**). The sizes of ZnO nanorod arrays could be controlled by tuning the reaction time and the concentration of the ammonia aqueous solution. ZnO nanorod array sensor has both high sensitivity to ammonia and reversibility at room temperature (25°C). And the response could be kept at least 5 days when the current intensity reduced to 50% of maximum.

## 2.5 Spray pyrolysis

ZnO nanorods with different sizes of hexagonal pillar shape have been successfully synthesized by spray pyrolysis technique (SPT). Zinc acetate solution was obtained by dissolving zinc acetate dihydrate in the mixture of methanol and double distilled water. During spray pyrolysis process, the precursor solution droplets close to the preheated substrates thermally decomposed and formed the highly adherent zinc oxide film. During the pyrolytic process, the following reaction takes place.



Highly uniform crystalline films were obtained upon the post deposition annealing at 500°C for 1 h in air. The spray pyrolysis setup used is schematically illustrated in **Figure 4**. The thin films comprise well-shaped hexagonal ZnO nanorods with a diameter of 90–120 nm and length of up to 200 nm. The gas-sensing properties of these films toward gases such as ethanol, CO<sub>2</sub>, NH<sub>3</sub>, CO, and H<sub>2</sub>S exposure have been investigated at operating temperature from 30 (room temperature) to 450°C. The ZnO nanorods thin films showed much better sensitivity and stability to H<sub>2</sub>S gas (100 ppm) at 50°C than the conventional ZnO materials without nanostructures [19].

## 2.6 Sonochemical route

A sonochemical route provides an effective way to grow vertically aligned ZnO nanorod arrays on a Pt-electrode patterned alumina substrate under ambient conditions [20]. **Figure 5(a)** shows the sensor substrate with the interdigitated

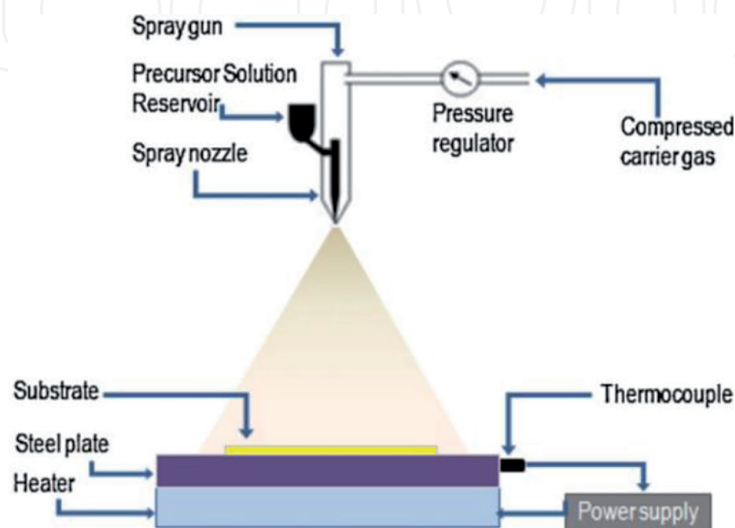


**Figure 4.**  
The scheme of the spray pyrolysis setup.

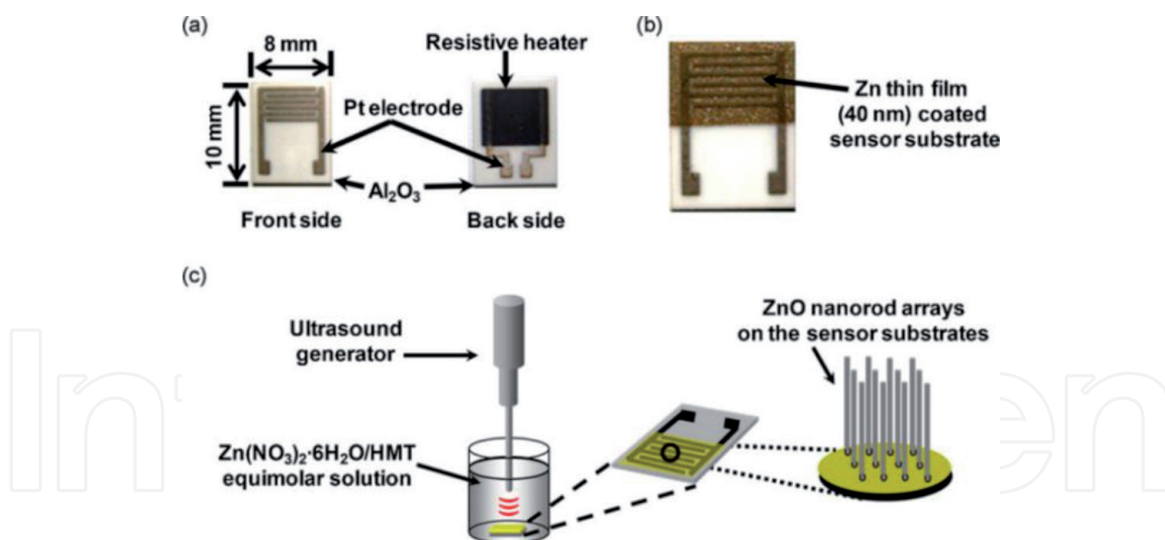


**Figure 5.**

(a) Photograph of sensor substrate including interdigitated comblike Pt electrodes and a resistive heater. (b) Zn thin-film sputtered sensor substrate. (c) A schematic illustration for the sonochemical growth of vertically aligned ZnO nanorod arrays on a sensor substrate.

comblike Pt electrodes on the front side and a resistive heater on the back. Upon the deposition of Zn thin film (40 nm) on the interdigitated Pt electrodes using RF sputtering technique as shown in **Figure 5(b)**, the sensor substrate was immersed in a mixed aqueous solution of  $\text{Zn}(\text{NO}_3)_2 \cdot 6\text{H}_2\text{O}$  and  $(\text{CH}_2)_6\text{N}_4$ . Ultrasonic waves at an intensity of  $39.5 \text{ W/cm}^2$  were introduced in the solution for 1 h. **Figure 5(c)** shows the scheme of the sonochemical growth of vertically aligned ZnO nanorod arrays on the substrate. The ZnO nanorods have the average diameter of 50 nm and length of 500 nm. The gas sensor based on sonochemically grown ZnO nanorod has high sensitivity to  $\text{NO}_2$  gas with a very low detection limit of 10 ppb at  $250^\circ\text{C}$  and short response and recovery time.

## 2.7 Simple solution route

Dodecyl benzene sulfonic acid sodium salt (DBS) was used as a modifying agent in a simple solution route to fabricate well-crystallized ZnO nanorods [21]. Zinc acetate dihydrate [ $\text{Zn}(\text{AC})_2 \cdot 2\text{H}_2\text{O}$ ] and DBS with a ratio of 1:8.5 were dissolved in a mixed solvent of ethylene glycol and xylene. Then a hydrazine monohydrate ethanol solution was drop-wisely introduced into the solution. After the reaction completed, the mixture was subsequently heated to boiling point ( $140^\circ\text{C}$ ) and refluxed. The resulting products were cooled down naturally, washed, and finally dried in the vacuum at  $70^\circ\text{C}$ . The ZnO nanorods sensors are highly sensitive and selective to TEA at low concentration of 0.001–1000 ppm among the gases of toluene, ethanol, benzene, and acetone. The prepared ZnO sensors to TEA exhibit high selectivity and superior sensitivity with the response of 6–0.001 ppm TEA at  $150^\circ\text{C}$ .

## 3. Controllable fabrication of ZnO nanorods

### 3.1 Growth control

The growth characteristics of the ZnO nanorod arrays (ZNAs) deposited using a wet chemical route were affected by several parameters, such as zinc seed layer morphology, zinc ion concentration, solution pH, deposition time, and growth temperature [7]. The surface and the cross-sectional FESEM images of the ZnO

nanorod films prepared with different growth times were shown in **Figure 6**. The length/diameter aspect ratio of the ZNAs also increased as the reaction time is extended [**Figure 6(a)** and **(c)**]. With the prolonged deposition time, upright and wider nanorods can be produced, but the nanorods easily merge with each other as they grow longer. The alignment of the nanorods in **Figure 6(a3)**, **(b3)**, and **(c3)** changes as the growth time is prolonged.

The length and inter-rod space have important influence on the gas-sensing performance of the devices. The ZnO:6 nanorods sample has small length and quite large spacing between them. However, both the length and the inter-rod spacing of the ZnO:9 nanorods samples are adequate and beneficial for the sensing performance. Nevertheless, for the ZnO:12 sample, the interspaces between nanorods are smallest due to the overlap between the nanorods. The gas sensors with ZnO:9 nanorod samples exhibits a high sensitivity of 3100% toward 100 ppm NO<sub>2</sub> at 175°C.

### 3.2 Selective growth

Selective growth of ZnO nanorod arrays with well-defined areas was developed to fabricate the NO<sub>2</sub> gas sensor. The seed layer was created by ink-jetting the seed solution on the interdigitated electrodes. Then, vertically aligned ZnO nanorods were grown by the hydrothermal approach on the patterned seed layer. The effects of the seed solution properties and the ink-jet printing parameters on the printing performance and the morphology of the nanorods were investigated [22].

FESEM images in **Figure 7** show the morphology of patterned ZnO nanorod films. ZnO nanorods are selectively grown on a round grown area with a diameter of 650 μm as shown in **Figure 7(a)**. **Figure 7(b)** and **(c)** present the enlarged edge images of the grown area. In **Figure 7(c)** the ZnO nanorod were selectively grown in a direction perpendicular to the substrate to produce vertically aligned arrays

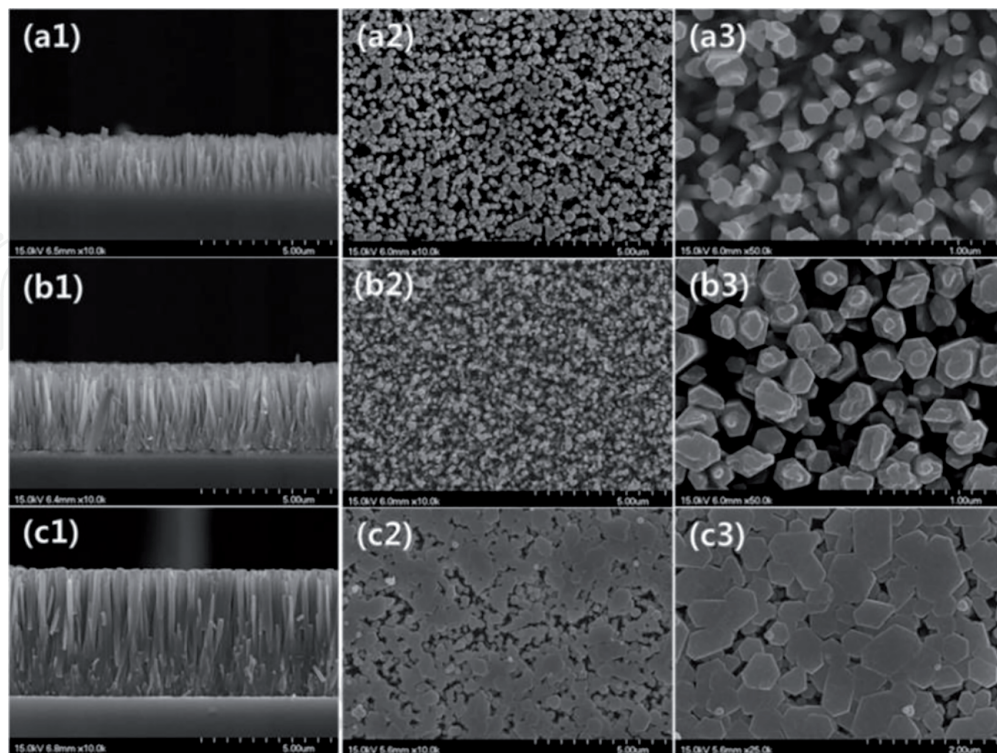


**Figure 6.** FESEM images of ZnO thin-film sample ZnO:6 to ZnO:12 (a1, a2, and a3) show cross-sectional view of ZnO:6, ZnO:9, and ZnO:12, respectively. a2, a3, b2, b3, c2, and c3 reveal low- and high-magnification FESEM images of ZnO thin-film sample ZnO:6 to ZnO:12.

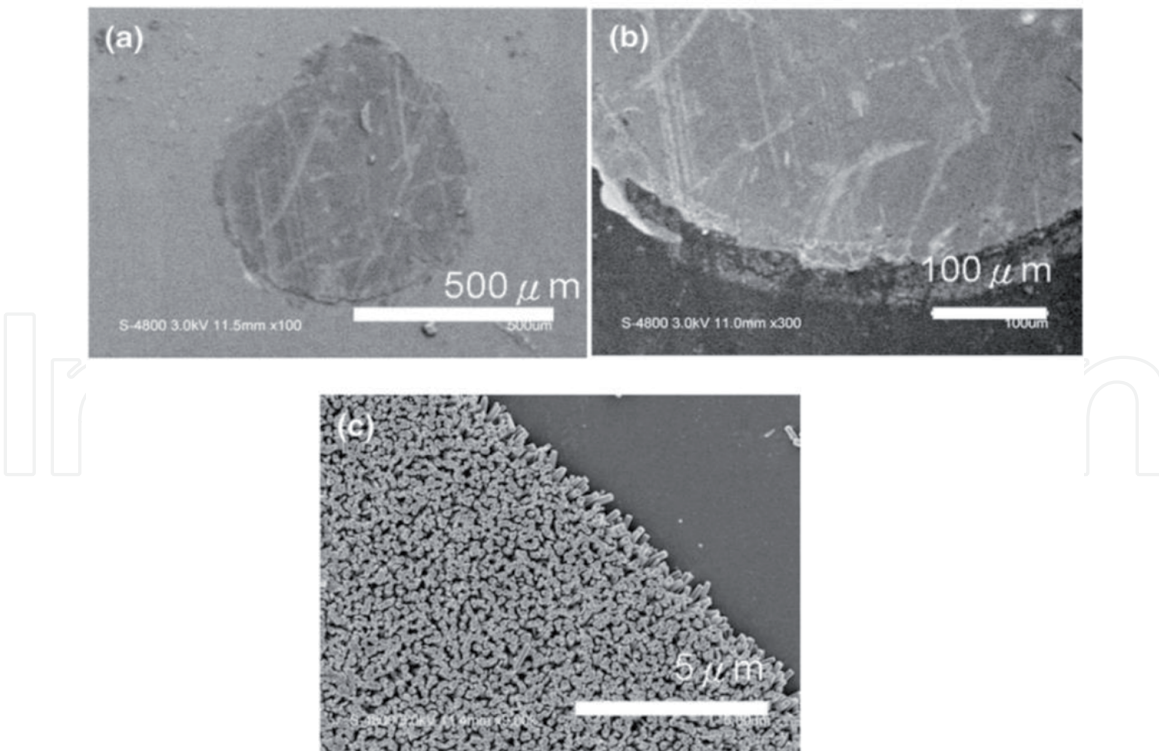


**Figure 7.** FESEM images of the selective grown ZnO nanorods micropattern: (a) entire pattern, (b) edges of the grown area, and (c) enlarged images of the nanorods.

of ZnO nanorods on the patterned area. Such a nanorod-array structure with high surface-to-volume ratio favors the adsorption and desorption of  $\text{NO}_2$  gas on the sensor.

The influence of different rod growth times on the morphology of ZnO nanorod films was investigated by FESEM with cross-sectional images illustrated in **Figure 8**. The ZnO nanorods become longer but the diameters of the nanorods nearly keep constant with the extension of the growth time. For example, the lengths of the ZnO nanorods grown for 2 and 4 h are 500 and 1300 nm, respectively, but their diameters are nearly the same in the range of 50–80 nm for both cases. Nanorod morphology has strong influence on the response performance of the sensor. The increasing nanorod aspect ratio increases the nanorod surface area and thus allows more gas adsorption interface. Larger fraction of the nanorod is depleted upon adsorption of  $\text{NO}_2$ . Longer growth time of the ZnO nanorod sensor results in longer nanorod so that the corresponding sensor has higher sensitivity than that with shorter growth time.

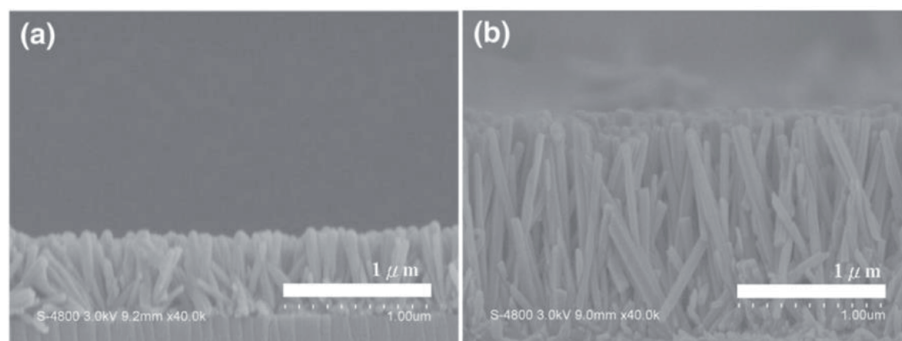


**Figure 8.** FESEM images of the cross section of ZnO nanorods prepared with different rod growth time (a) 2 h and (b) 4 h.

### 3.3 Diameter regulation

The size (diameter or length) of ZnO nanorods grown via hydrothermal method is affected by several factors such as concentration of precursors, growth temperature, and time. The average diameter of ZnO nanorods can be regulated by changing growth time. The average diameter is about 35 nm with the growth time of 0.5 h. Upon the growth time over 1 h, the average diameter rapidly increases up to 100 nm when the growth time is 2.5 h. But then the average diameter keeps nearly constant as the growth time is elongated [23]. ZnO nanorod arrays were successfully synthesized on Si substrates using two-step route including spin-coating seed on substrates and chemical bath deposition (CBD) growth. The diameter of ZnO nanorods can be controlled by changing seed density on substrates or NaOH concentration in solution. Increasing spin-coating times leads to better seed density so that the diameter of ZnO nanorods decreases from 150 to 70 nm as the spin-coating times increase from 1 to 50. And the diameter of ZnO nanorods obviously increases with NaOH concentration increasing [24].

Solvent polarity has a special effect on final dimension of the ZnO nanorods synthesized using a one-step solvothermal method. The diameter of ZnO nanorods decreased with the moderated polarity by introducing less polar ethanol solvent. The diameter of the ZnO nanorods can be regulated by adjusting ethanol content in the solvent in that the diameter of the ZnO nanorods decreases as ethanol content in the solution increases. **Figure 9** shows SEM images of samples a0, a10, a20, a30, a40, and a50 prepared by introducing 0, 10, 20, 30, 40, and 50 vol% ethanol solvent, respectively. **Figure 9(a)** shows ZnO nanorod surface full of flocs when

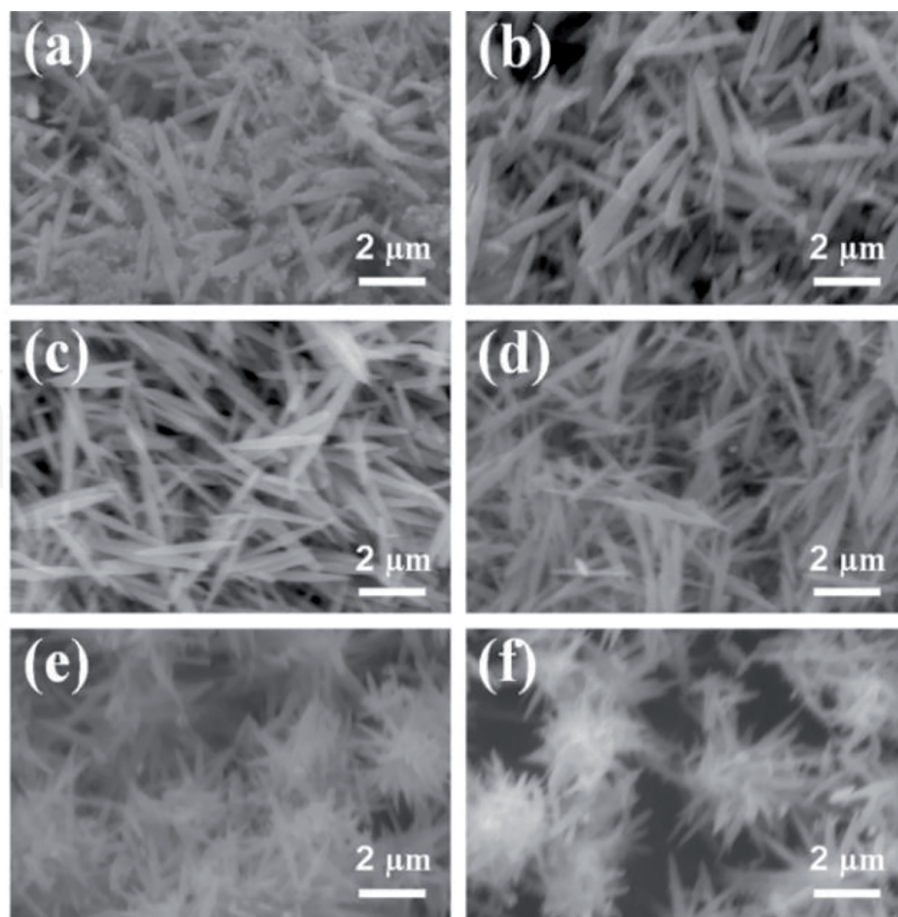


**Figure 9.** SEM images of ZnO nanorod samples (a) a0, (b) a10, (c) a20, (d) a30, (e) a40, and (f) a50 prepared with 0, 10, 20, 30, 40, and 50 vol% ethanol solvent.

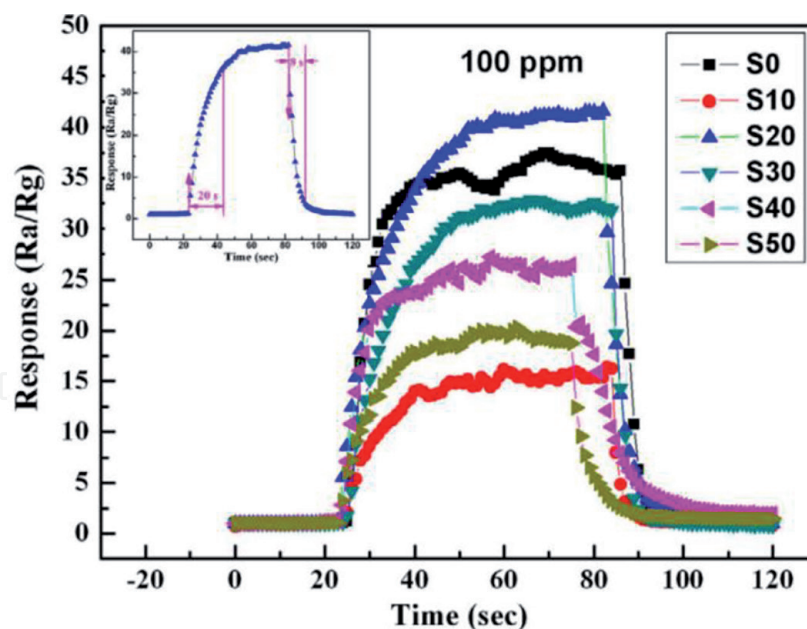


**Figure 10.** Response and recovery curves toward 100 ppm ethanol at the optimum working temperature of 370°C.

prepared in pure water solvent. The flocs disappeared upon the addition of 10 vol% ethanol, as shown in **Figure 9(b)**. When ethanol was increased to 20 vol% (**Figure 9(c)**) and 30 vol% (**Figure 9(d)**), ZnO nanorods show uniform, well-defined, and well-dispersed morphologies. The average nanorod diameter decreased from 360 to 220 nm when ethanol percentage in solvent increased from 10 to 50%.

**Figure 10** shows transient response and recovery curves of the ZnO nanorod sensors toward 100 ppm alcohol vapor at the optimum working temperature of 370°C. Here the sensors fabricated using samples a0, a10, a20, a30, a40, and a50 are labeled as S0, S10, S20, S30, S40, and S50, respectively. It is apparent that S20 is much superior to others. The inset with a single response and recovery curve of S20 measured at the same condition indicates that its sensor has the response of 42 and very sharp response and recovery time of 20 and 8 s, respectively [25].

## 4. Different structures formed by ZnO nanorods

### 4.1 Cross-linked configuration

Ammonia sensors based on ZnO nanorods (NRs) with a cross-linked configuration has excellent sensing performance by shrinking the interdigitated electrode spacing  $d$ . The electrode spacing  $d$ , working temperature, and gas concentration strongly influence the steady- and dynamic-responses and the related repeatability and different gaseous response performance [26]. Reducing the electrode spacing  $d$  increased the ammonia sensor response  $S$  because the configuration of ZnO NRs is transformed. The studied sensor with an electrode spacing  $d$  of 2  $\mu\text{m}$  at 573 K shows a highest ammonia sensor response  $S$  of 81.6 toward 1000 ppm  $\text{NH}_3/\text{air}$  gas and could detect  $\text{NH}_3/\text{air}$  with a lower ammonia concentration of 10 ppm. Moreover, the response  $S$  of the ammonia sensor is temperature dependent, as is mainly attributed to reactions of oxygen species. The adsorption-time ( $\tau_a$ ) and desorption-time ( $\tau_b$ ) constants of the studied sensor ( $d = 2 \mu\text{m}$ ) at 573 K are less than 3 min. The improvement of ammonia-sensing ability could result from the formation of more cross-linked configurations. Finally, the studied sensor with a cross-linked configurations shows good ammonia gas-sensing response and repeatability.

## 4.2 Flowerlike structures

Rather vertically aligned ZnO rods with flowerlike structures synthesized via carbothermal reduction vapor phase transport (CTR-VPT) method exhibited good crystallinity with preferential c-axis orientation and considerable quantity of oxygen vacancy [27]. **Figure 11** shows the ZnO nanorods have diameter in the range of 300–500 nm and length in the range of 7–9.5  $\mu\text{m}$ . In this configuration, a porous network formed by nanorods consists of directional channels for gas diffusion in and out. The interconnected nanorods provide a continuous electrical path for carrier transport between the two gold electrodes. The flowerlike bundle of rods increases the effective surface area and thus enhances gas sensitivity. The  $\text{H}_2\text{S}$  sensor with the ZnO nanorods of the flowerlike structure exhibits a high response (e.g.,  $S = 296$  at 1 ppm and 581 at 5 ppm) and good selectivity at room temperature and 250°C. However, the response and recovery times decreased with the increasing temperature.

## 4.3 Multishelled hollow spheres

ZnO with multishelled hollow spheres of 5  $\mu\text{m}$  in diameter were prepared by a facile solvothermal process in a ternary solvent system. The anisotropic single-crystalline nanorod building blocks with uniform diameter of about 40 nm are highly directional in the as-synthesized products. The evolution process of hollow ZnO core-shell structures consists of a two-step self-assembly process and symmetric Ostwald ripening starting from the inner core and at the interface of the core and shell. The hollow spheres and core-shell structures could be obtained by simply adjusting the composition of the mixed solvents, as is critical to the packing design [28]. In comparison of the hollow structures and nanorods at all working temperatures, the double-wall hollow structures exhibited the highest sensitivity to formaldehyde gas due to the high donor-related (DL) and the low acceptor-related

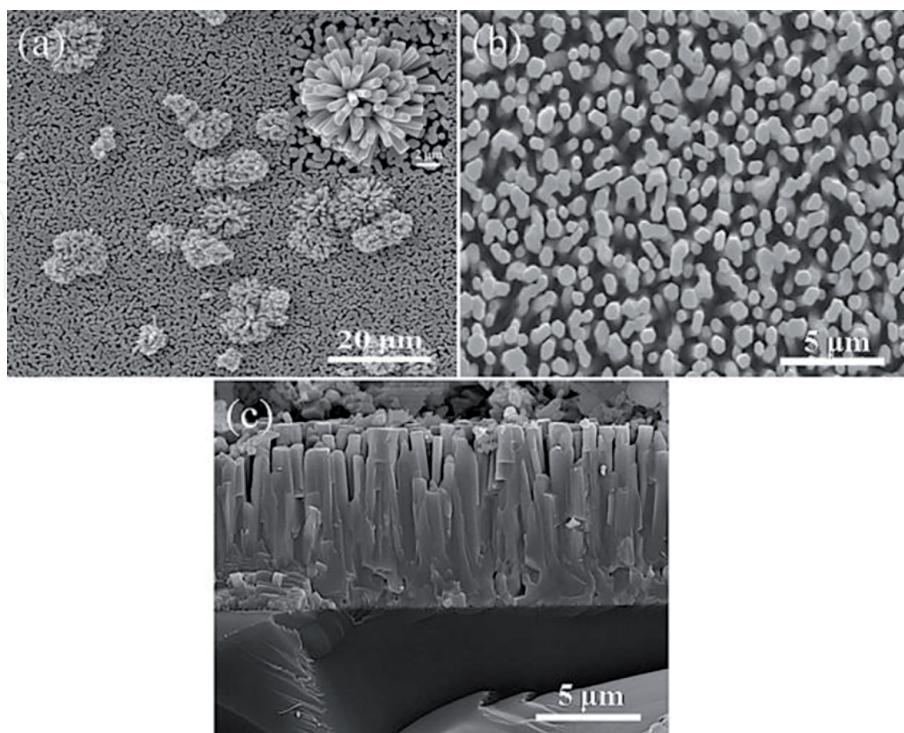


**Figure 11.** (a and b) Typical top view and (c) cross-sectional SEM images of the vertically aligned ZnO rods with flowerlike structures. Inset of **Figure 10(a)** shows magnified image of one of the flowers.

(AL) intrinsic defects. ZnO semiconductor with high response and selectivity to H<sub>2</sub>S as well as good stability was obtained by controlling the shape-defined building units and their assembly structure.

#### 4.4 Hollow microhemispheres

Self-assembling ZnO nanorods into 3D ZnO hollow microhemispheres is simply done by solvothermal reaction of zinc and alkali source in the presence of ethylene glycol. The 3D ZnO hollow microhemispheres were synthesized by the primary formation of glycolate precursors and subsequent transformation into ZnO. Glycol such as EG and the solvothermal process play the critical role in the synthesis. Numerous orderly and radical nanorods in the 3D ZnO hollow microhemispheres have the diameter of about 50 nm and length of several hundred nanometers. Furthermore, high sensitivity for ethanol and ammonia as well as quick response and recovery time at room temperature were obtained for the 3D ZnO hollow microhemisphere-based gas sensor due to the high surface-to-volume ratio [29].

### 5. Modification of ZnO nanorods

#### 5.1 Doping

The ZnO-sensing performance can be effectively improved by doping with transition metal elements. Vertically aligned yttrium-doped ZnO nanorod (YZO NR) arrays were synthesized by a one-pot hydrothermal method [30]. The Y doping concentration strongly influences the surface morphology of the NRs. With the dopant concentration increasing, longer and sharper NRs with high aspect ratio formed, and the aspect ratio of the YZO NRs was increased from 11 to 25. The Y doping reduced the ZnO NR resistivity to its minimum by a factor of 115 for the Y<sub>0.10</sub>ZnO. And the corresponding sensor gave the highest sensitivity toward all the tested gas species with the lowest breakdown voltage. The sensitivity of the sensor based on Y-doped ZnO nanorod arrays was enhanced up to sixfold, and the breakdown voltage from the highly conductive YZO NRs significantly reduced. The Cr-doped ZnO sensor presents the response of 104 to 100 ppm acetone at 300°C, as is four times higher than that of ZnO sensor. The increase of electron concentration optimized by Cr doping improved the sensing response and selectivity [31].

#### 5.2 Functionalization

The sensitivity and responding kinetics of metal oxide semiconductors (MOS) can be improved by the surface functionalization with noble metal NPs (e.g., Pd, Au, and Pt) because it provides the preferred adsorption and activation sites for the target analyte to react with the ionosorbed oxygen. CuO with a low band gap of 1.2–2.0 eV is a p-type semiconductor and can form p-n junctions with n-type metal oxides to extend the space-charge region, as locally narrows the conducting channel for the charge carriers in the ZnO. The p-n junction is thus more sensitive to gas molecule-induced charge transfer, and the gas-sensing selectivity and sensitivity is improved. CuO-functionalized ZnO nanorods were synthesized by a chemical bath deposition method. And their sensor showed enhanced gas response compared with bare ZnO NRs. According to both a collective- and a local-site approach, the deposition of CuO altered the overall band structure and surface properties of the ZnO [32].

### 5.3 Decoration

Pd-decorated ZnO nanorod structures were fabricated by sputter depositing Pd on the hydrothermally grown ZnO nanorods and the subsequent oxidation for detecting H<sub>2</sub>S gas at room temperature. The dissociation of H<sub>2</sub>S gas molecules on Pd accelerated, as facilitated the room temperature-sensing capability [33]. Therefore, the Pd decoration enhanced the sensing response to H<sub>2</sub>S at the examined operation temperatures. **Figure 12(a)** shows higher response level of ZnO:Pd nanorod structure than the ZnO nanorod structure at 300°C. **Figure 12(b)** shows a more dramatic effect of Pd at room temperature because the response of the ZnO:Pd sensor to 500 ppm H<sub>2</sub>S is approximately ~16% compared with the pure ZnO nanorod of no H<sub>2</sub>S-sensing response at RT. The Pd-decorated ZnO nanorods showed a stable performance as well as good stability and repeatability. The response time was approximately 12 min, but the recovery time was much longer, approximately 10 h. Moreover, the CaO-decorated n-ZnO nanorods showed stronger response to NO<sub>2</sub> than the pristine ZnO nanorods [34].

### 5.4 Sensitization

The sensitivity and the selectivity of the sensor can be improved by different strategies such as incorporating dopants, applying ultraviolet (UV) irradiation, and sensitizing the sensing layer with noble metals (Au, Pt, Pd) and metal oxides (CuO, SnO<sub>2</sub>). It is known that sensitizing the sensing layer by noble metals is most

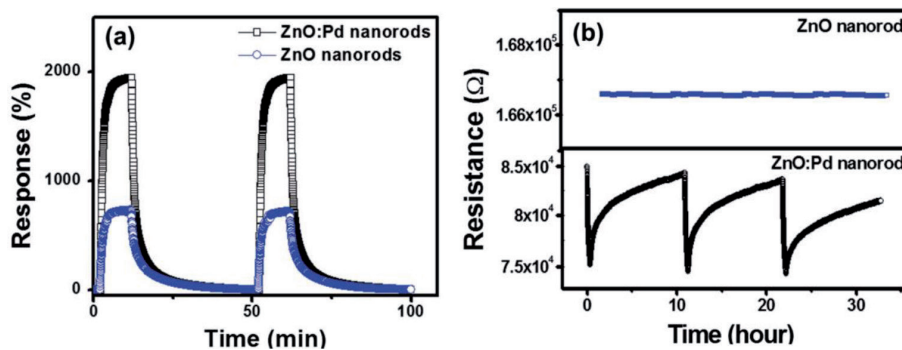


**Figure 12.** Comparison of H<sub>2</sub>S sensing between ZnO and ZnO:Pd nanorod structures at (a) 300°C and (b) room temperature.

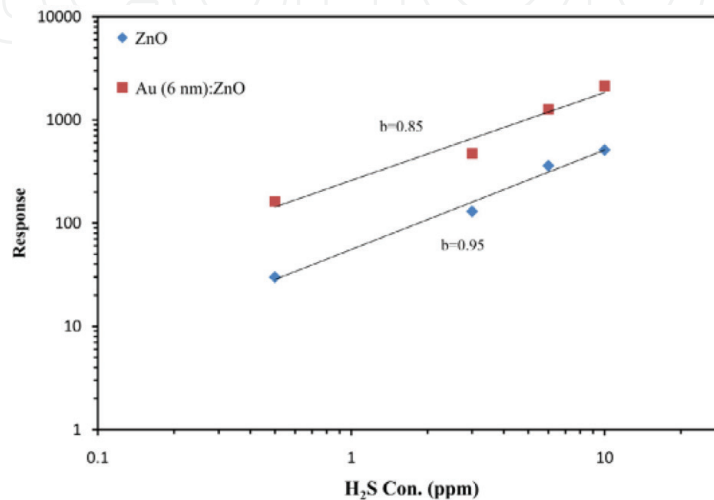


**Figure 13.** Response of sensors based on pure and Au-modified ZnO samples versus different concentrations of H<sub>2</sub>S gas.

effective. The sputter deposition of Au layer with different nominal thicknesses on ZnO nanorods enhanced the sensing response to H<sub>2</sub>S at room temperature (25°C). When Au layer with 6 nm nominal thickness is deposited, higher response and selectivity to H<sub>2</sub>S than those reported in the literature are obtained. The sensing response at room temperature was enhanced because Au islands formed Schottky barriers at Au-ZnO interface, introduced surface active sites, and increased effective surface area through surface coarsening. The response of both pure and Au-sensitized rods increases with the gas concentration as shown in **Figure 13**. The fabricated sensor based on the Au-sensitized ZnO nanorods is able to detect H<sub>2</sub>S gas of ppb level [1].

## 6. ZnO nanorod-based composites

### 6.1 ZnO@ZIF-8 core-shell nanorod film

**Figure 14** shows ZnO@ZIF-8 (zeolitic imidazolate framework-8) core-shell nanorod film was designed and synthesized through a facile solution deposition method for H<sub>2</sub> gas sensor. The ZnO@ZIF-8 core-shell nanorod film with a thin, fine-grain, porous ZIF-8 shell realized the selective response for H<sub>2</sub> over CO and enhances the H<sub>2</sub> sensitivity [35]. The 2-methylimidazole (HmIM) concentration plays a crucial role in forming the core-shell structure and controlling the ZIF-8 grain size. The H<sub>2</sub>O/DMF volume ratio influenced the integrity of the core-shell structure, and the reaction time affects its continuity. The introduction of more oxygen vacancies to the ZnO@ZIF-8 core-shell nanorod film enhanced H<sub>2</sub> sensitivity in comparison with the raw ZnO nanorod film. The ZnO@ZIF-8 core-shell nanorod film has highly porous microstructure owing to the contribution of the ZIF-8 shell. The strengthened molecular sieving effect of the ZIF-8 shell because of its fine-grain (<140 nm) structure resulted in no response for CO for the ZnO@ZIF-8 core-shell nanorod film. The selective response of H<sub>2</sub> over CO was realized by the integration of ZnO with ZIF-8 and the control of their microstructures.

### 6.2 ZnO/MWNTs hierarchical nanostructure

ZnO/multiwall carbon nanotubes (MWNTs) composite with a hierarchical nanostructure was fabricated using layer-by-layer self-assembly technique. The

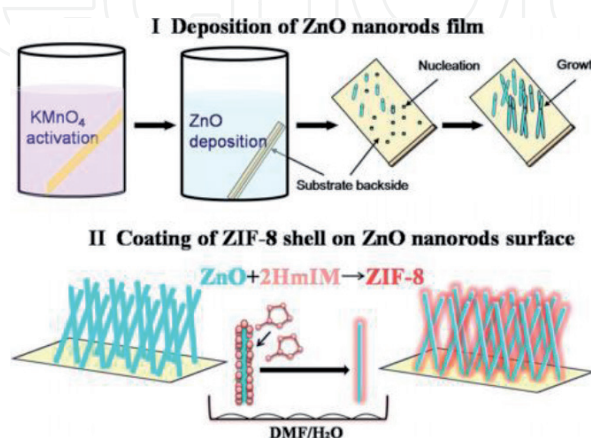


**Figure 14.**

Formation process of ZnO@ZIF-8 core-shell nanorod films: (I) ZnO nanorod films were deposited on the KMnO<sub>4</sub>-activated substrates; (II) ZnO@ZIF-8 core-shell nanorod films were fabricated by immersing the ZnO nanorod films into the 2-methylimidazole (HmIM) solution [the solvent contained H<sub>2</sub>O and N,N-dimethylformamide (DMF)].

as-prepared ZnO was nanorod-shaped crystal in **Figure 15(a)**. **Figure 15(b)** indicates the interdigitated or interweaved MWNTs with a random network structure. **Figure 15(c)** shows that the ZnO/MWNTs film comprised ZnO nanorods and MWNTs wrapped closely together. **Figure 15(d)** shows the XRD spectra of ZnO, MWNTs, and ZnO/MWNTs film. A peak at 2 $\theta$  angle of 25.18 occurred in the XRD pattern of MWNTs and major peaks at 2 $\theta$  angle of 24.72, and 31.78 were observed in the XRD patterns of ZnO/MWNTs nanocomposite.

**Figure 16** compared the gas-sensing properties of pure ZnO sensor, ZnO/PSS and ZnO/MWNTs sensors tested under the same experimental environment toward 5–500 ppm ethanol gas concentration. The sensing properties of the ZnO/MWNTs nanocomposite sensor were significantly superior to those of pure ZnO sensor and ZnO/PSS nanocomposite sensor. For instance, pure ZnO, ZnO/PSS, and ZnO/MWNTs sensors have the normalized response values of 2.6, 3, and 4.5% to 50 ppm ethanol gas, respectively.

Furthermore, **Figure 17** compares the response and recovery characteristics for the three sensors exposed to 50 ppm ethanol gas. ZnO, ZnO/PSS, and ZnO/MWNTs sensor exhibits the response time of 13, 11, and 7 s and the recovery time of 17, 19, and 11 s for, respectively. The response and recovery time of ZnO/MWNTs sensor is much shorter than those of the other two sensors. Therefore, the ZnO/MWNTs film sensor exhibited more outstanding sensitivity, prompter response recovery time and better repeatability than the other two sensors [36].

### 6.3 Fe<sub>2</sub>O<sub>3</sub>/ZnO core-shell nanorods

Fe<sub>2</sub>O<sub>3</sub>/ZnO core-shell nanorods prepared by hydrolysis method [37] have higher surface area than bulk ZnO sensor materials. High response, good stability, and short response/recovery time were obtained for the resultant Fe<sub>2</sub>O<sub>3</sub>/ZnO gas sensor to detect low concentrations of various combustible gases. The ZnO shell of about 2–3 nm was coated on the surface of Fe<sub>2</sub>O<sub>3</sub> nanorods and much thinner than the conventional ZnO-based sensor devices. The response/recovery time was less

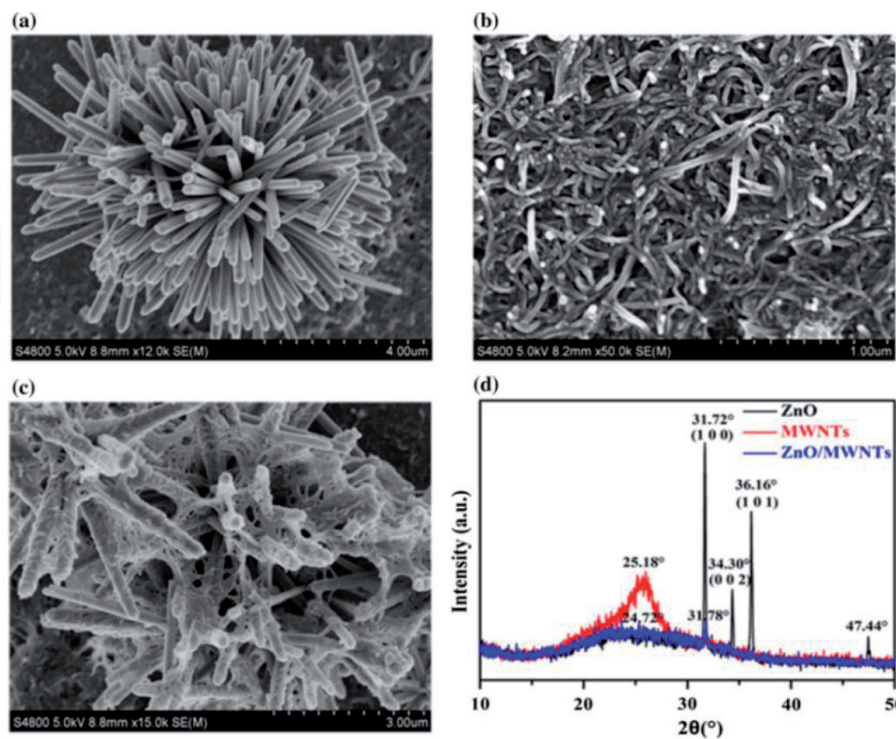


**Figure 15.** SEM images of ZnO film (a), MWNTs film (b), and ZnO/MWNTs film (c) and XRD observation of ZnO, MWNTs, and ZnO/MWNTs films (d).

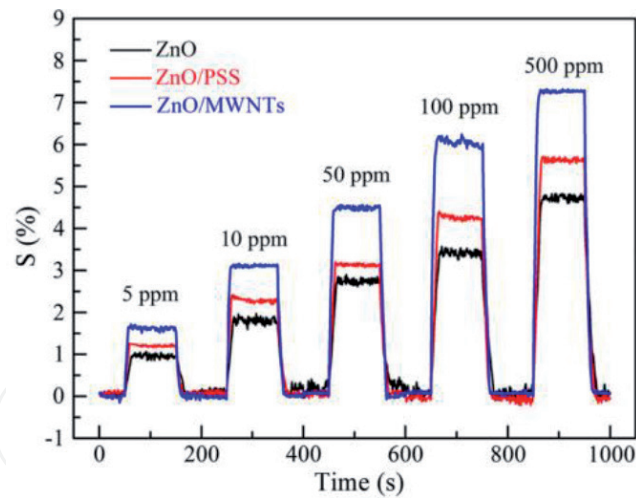


**Figure 16.**

*Normalized response of ZnO, ZnO/PSS, and ZnO/MWNTs film sensors to various ethanol concentrations.*

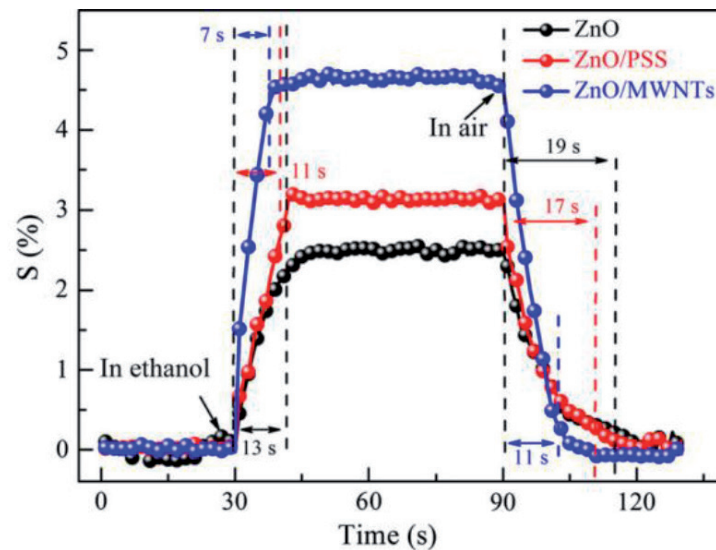


**Figure 17.**

*The response and recovery characteristics of ZnO, ZnO/PSS, and ZnO/MWNTs film sensors exposed to 50 ppm ethanol gas at room temperature.*

than 20 s, and the response slightly decreased after 4 months. The present  $\text{Fe}_2\text{O}_3/\text{ZnO}$  core-shell nanorods with these favorable gas-sensing features are particularly attractive as a promising practical sensor.

#### 6.4 $\text{Ga}_2\text{O}_3$ -core/ $\text{ZnO}$ -shell nanorods

$\text{Ga}_2\text{O}_3$ -core/ $\text{ZnO}$ -shell nanorods were fabricated by the thermal evaporation of GaN powders and subsequent atomic layer deposition of ZnO [38]. The diameter of the nanorods ranges from a few tens to a few hundreds of nanometers, and their length is up to a few hundreds of micrometers. The cores of the nanorods were single crystal monoclinic  $\text{Ga}_2\text{O}_3$ , and their shells were single crystal ZnO. The sensors based on multiple networked  $\text{Ga}_2\text{O}_3$ -core/ $\text{ZnO}$ -shell nanorods showed responses of 7247, 21,352, 32,778, and 27,347% (181, 474, 692, and 355 times larger than those of bare- $\text{Ga}_2\text{O}_3$  nanorod sensors) at  $\text{NO}_2$  concentrations of 10, 50, 100, and 200 ppm, respectively, at  $300^\circ\text{C}$ . The core-shell nanorods have much better response to  $\text{NO}_2$  gas than the other material nanosensors reported previously.  $\text{Ga}_2\text{O}_3$  nanorods encapsulated by ZnO exhibits substantial improvement in the response to  $\text{NO}_2$  gas,

as can be explained by the space-charge model. The  $\text{Ga}_2\text{O}_3\text{-ZnO}$  heterojunction facilitates or restrains electron transfer as a lever and enhances the sensing properties of the core-shell nanorod sensor. Moreover, the recovery time of the core-shell nanorods was almost 1/3 that of the bare- $\text{Ga}_2\text{O}_3$  nanorods at a  $\text{NO}_2$  concentration of 10 ppm and almost a half at other  $\text{NO}_2$  concentrations, even if the response time of the former is longer than that of the latter.

### 6.5 $\text{In}_2\text{O}_3\text{-core/ZnO-shell}$ nanorods

The two-step fabrication process of  $\text{In}_2\text{O}_3\text{-core/ZnO-shell}$  nanorods comprises the thermal evaporation of a 1:1 mixture of  $\text{In}_2\text{O}_3$  and graphite powders and the atomic layer deposition of ZnO [39]. The core-shell nanorods have the diameter in the range of 100–200 nm and the length up to a few hundreds of micrometers. The thickness of the ZnO-shell layer in the core-shell nanorod ranged from 5 to 10 nm. The nanorods consist of bcc-structured polycrystalline  $\text{In}_2\text{O}_3$  as cores and simple hexagonal-structured polycrystalline ZnO as shells. The responses of the multiple networked  $\text{In}_2\text{O}_3\text{-core/ZnO-shell}$  nanorod sensors at  $\text{H}_2\text{S}$  concentrations of 10, 25, 50, and 100 ppm were 34.11, 34.55, 35.77, and 28.86%, respectively, at 300°C and 4.2, 4.0, 4.0, and 3.5 times larger than those of bare- $\text{In}_2\text{O}_3$  nanorod sensors, respectively. Based on the space-charge model, the  $\text{In}_2\text{O}_3\text{-ZnO}$  heterojunction acts as a lever to facilitate or restrain the electron transfer and thus enhances the sensing properties of the core-shell nanorod sensor. In addition, the  $\text{In}_2\text{O}_3\text{-core/ZnO-shell}$  nanorods sensor exhibits shorter response and recovery times than the bare- $\text{In}_2\text{O}_3$  nanorods for any  $\text{H}_2\text{S}$  concentration.

### 6.6 ZnO NRs-Gr/M hybrid architectures

The ZnO nanorods (NRs) and graphene (Gr) (ZnO NRs-Gr/M) hybrid architectures fabricated in **Figure 18** [40] accommodated the flexural deformation without mechanical or electrical failure for bending radius below 0.8 cm under the repeated bending and releasing up to 100 times. Furthermore, the gas sensors can detect ethanol gas vapor at the ppm level with the sensitivity (resistance in air/resistance in target gas) as high as  $\sim 9$  for 10 ppm ethanol. The combination of 1D nanocrystals

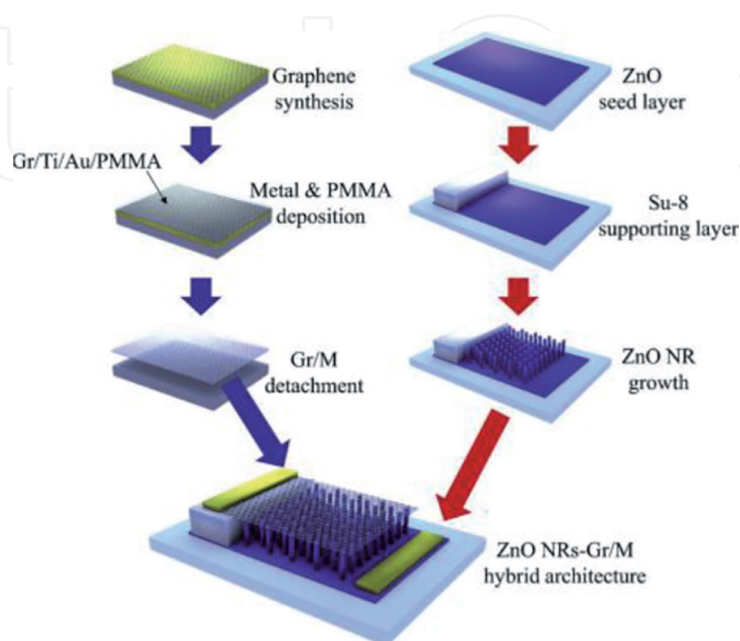


**Figure 18.** Schematic illustration of the key steps for fabricating the ZnO NRs-Gr/M hybrid architectures.

and 2D Gr improves the performances of the sensors and also imposes additional mechanical functions to the devices.

## 7. Conclusions and future outlooks

In this chapter, ZnO nanorods for gas sensors were reviewed. ZnO nanorods with various kinds of morphology were synthesized by different fabrication methods. Their synthesis processes including some reaction formula were introduced, and the sensing properties such as fast response, high responsibility, and good stability were described. Furthermore, the growth of ZnO nanorods can be controlled by tuning the reaction parameters. ZnO nanorods were selectively grown on the seed layer, and their morphology was influenced by the rod growth time. The diameter of ZnO nanorods can be regulated by the solution concentration, the growth time, and the seed density. The ZnO nanorods can form different special structures, and their improvement of the sensing properties was explained from a microscopic point of view. For instance, the flowerlike structure of ZnO nanorods increases the effective surface area and thus enhances gas sensitivity. The sensing performance can be effectively improved by doping with transition metal elements, surface functionalization with noble metals, and decoration with Pd or CaO. Finally, the core-shell nanorods composite based on ZnO, hierarchical nanostructure ZnO/MWCNTs composite, and ZnO nanorods-Gr/M hybrid architectures combine the advantages of both components and improve the performance of the sensors. In the future, novel fabrication methods, further modification, and more composites with different materials are perspectives for the sensors based on ZnO nanorods. The sensing properties such as responsibility and stability need to be improved for the practical application. Moreover, the sensing mechanism of the ZnO nanorods sensors is unclear and necessary to be declared. In summary, great progress have been made on the research of ZnO nanorods for gas sensors; however, improvement area still exists for the further study.

IntechOpen

### Author details

Yanmin Wang

College of Materials Science and Engineering, Shandong University of Science and Technology, Qingdao, Shandong, P. R. China

\*Address all correspondence to: yanmin\_w@163.com

### IntechOpen

© 2020 The Author(s). Licensee IntechOpen. This chapter is distributed under the terms of the Creative Commons Attribution License (<http://creativecommons.org/licenses/by/3.0>), which permits unrestricted use, distribution, and reproduction in any medium, provided the original work is properly cited. 

## References

- [1] Hosseini ZS, Mortezaali A, Zad AI, Fardindoost S. Sensitive and selective room temperature H<sub>2</sub>S gas sensor based on Au sensitized vertical ZnO nanorods with flower-like structures. *Journal of Alloys and Compounds*. 2015;**628**:222-229. DOI: 10.1016/j.jallcom.2014.12.163
- [2] Yu L, Liu S, Yang B, Wei J, Lei M, Fan X. Sn-Ga Co-doped ZnO nanobelts fabricated by thermal evaporation and application to ethanol gas sensors. *Materials Letters*. 2015;**141**:79-82. DOI: 10.1016/j.matlet.2014.11.049
- [3] Hoefler U, Frank J, Fleischer M. High temperature Ga<sub>2</sub>O<sub>3</sub>-gas sensors and SnO<sub>2</sub>-gas sensors: a comparison. *Sensors and Actuators B*. 2001;**78**(1):6-11. DOI: 10.1016/S0925-4005(01)00784-5
- [4] Miller DR, Akbar SA, Morris PA. Nanoscale metal oxide-based heterojunctions for gas sensing: A review. *Sensors and Actuators B: Chemical*. 2014;**204**:250-272. DOI: 10.1016/j.snb.2014.07.074
- [5] Datta N, Ramgir N, Kaur M, Ganapathi SK, Debnath AK, Aswal DK, et al. Selective H<sub>2</sub>S sensing characteristics of hydrothermally grown ZnO-nanowires network tailored by ultrathin CuO layers. *Sensors and Actuators B*. 2012;**166-167**(6):394-401. DOI: 10.1016/j.snb.2012.02.079
- [6] Lv Y, Lin G, Xu H, Chu X. Gas-sensing properties of well-crystalline ZnO nanorods grown by a simple route. *Physica E: Low-dimensional Systems and Nanostructures*. 2007;**36**(1):102-105. DOI: 10.1016/j.physe.2006.09.014
- [7] Vanalakar SA, Patil VL, Harale NS, Vhanalakar SA, Gang MG, Jin YK, et al. Controlled growth of ZnO nanorod arrays via wet chemical route for NO<sub>2</sub> gas sensor applications. *Sensors and Actuators B: Chemical*. 2015;**221**:1195-1201. DOI: 10.1016/j.snb.2015.07.084
- [8] Seiyama T, Kato A, Fujiishi K, Nagatani M. A new detector for gaseous components using semiconductive thin films. *Analytical Chemistry*. 1966;**38**(8):1502-1503. DOI: 10.1021/ac60240a031
- [9] Li XB, Ma SY, Li FM, Chen Y, Zhang QQ, Yang XH, et al. Porous spheres-like ZnO nanostructure as sensitive gas sensors for acetone detection. *Materials Letters*. 2013;**100**(6):119-123. DOI: 10.1016/j.matlet.2013.02.117
- [10] Sonker RK, Sabhajeet SR, Singh S, Yadav BC. Synthesis of ZnO nanopetals and its application as NO<sub>2</sub> gas sensor. *Materials Letters*. 2015;**152**:189-191. DOI: 10.1016/j.matlet.2015.03.112
- [11] Jin WX, Ma SY, Tie ZZ, Xu XL, Jiang XH, Li WQ, et al. Synthesis of monodisperse ZnO hollow six-sided pyramids and their high gas-sensing properties. *Materials Letters*. 2015;**159**:102-105. DOI: 10.1016/j.matlet.2015.06.085
- [12] Luo J, Ma SY, Sun AM, Cheng L, Yang GJ, Wang T, et al. Ethanol sensing enhancement by optimizing ZnO nanostructure: From 1D nanorods to 3D nanoflower. *Materials Letters*. 2014;**137**:17-20. DOI: 10.1016/j.matlet.2014.08.108
- [13] Gurav KV, Deshmukh PR, Lokhande CD. LPG sensing properties of Pd-sensitized vertically aligned ZnO nanorods. *Sensors and Actuators B: Chemical*. 2011;**151**(2):365-369. DOI: 10.1016/j.snb.2010.08.012
- [14] Pawar RC, Shaikh JS, Suryavanshi SS, Patil PS. Growth of ZnO nanodisk, nanospindles and nanoflowers for gas sensor: Ph dependency. *Current Applied Physics*. 2012;**12**(3):778-783. DOI: 10.1016/j.cap.2011.11.005

- [15] Jiao M, Chien NV, Duy NV, Hoa ND, Hieu NV, Hjort K, et al. On-chip hydrothermal growth of ZnO nanorods at low temperature for highly selective NO<sub>2</sub> gas sensor. *Materials Letters*. 2016;**169**:231-235. DOI: 10.1016/j.matlet.2016.01.123
- [16] Lim SK, Hwang S-H, Kim S, Park H. Preparation of ZnO nanorods by microemulsion synthesis and their application as a CO gas sensor. *Sensors and Actuators B: Chemical*. 2011;**160**(1):94-98. DOI: 10.1016/j.snb.2011.07.018
- [17] Tan ST, Tan CH, Wu YC, Chi CY, Umar AA, Ginting RT, et al. Microwave-assisted hydrolysis preparation of highly crystalline ZnO nanorod array for room temperature photoluminescence-based CO gas sensor. *Sensors and Actuators B: Chemical*. 2016;**227**:S0925400515307851. DOI: 10.1016/j.snb.2015.12.058
- [18] Qiu Y, Yang M, Fan H, Xu Y, Shao Y, Yang X, et al. Synthesis of ZnO nanorod arrays on Zn substrates by a gas-solution-solid method and their application as an ammonia sensor. *Journal of Materials Science*. 2014;**49**(1):347-352. DOI: 10.1007/s10853-013-7711-0
- [19] Shinde SD, Patil GE, Kajale DD, Gaikwad VB, Jain GH. Synthesis of ZnO nanorods by spray pyrolysis for H<sub>2</sub>S gas sensor. *Journal of Alloys and Compounds*. 2012;**528**:109-114. DOI: 10.1016/j.jallcom.2012.03.020
- [20] Oh E, Choi H-Y, Jung S-H, Cho S, Kim JC, Lee K-H, et al. High-performance NO<sub>2</sub> gas sensor based on ZnO nanorod grown by ultrasonic irradiation. *Sensors and Actuators B: Chemical*. 2009;**141**(1):239-243. DOI: 10.1016/j.snb.2009.06.031
- [21] Lv YZ, Li CR, Guo L, Wang FC, Xu Y, Chu XF. Triethylamine gas sensor based on ZnO nanorods prepared by a simple solution route. *Sensors and Actuators B: Chemical*. 2009;**141**(1):85-88. DOI: 10.1016/j.snb.2009.06.033
- [22] Chang C-J, Hung S-T, Lin C-K, Chen C-Y, Kuo E-H. Selective growth of ZnO nanorods for gas sensors using ink-jet printing and hydrothermal processes. *Thin Solid Films*. 2010;**519**(5):1693-1698. DOI: 10.1016/j.tsf.2010.08.153
- [23] Yuan Z, Yu J, Wang N, Jiang Y. Well-aligned ZnO nanorod arrays from diameter-controlled growth and their application in inverted polymer solar cell. *Journal of Materials Science: Materials in Electronics*. 2011;**22**:1730-1735. DOI: 10.1007/s10854-011-0353-6
- [24] Li X, Wang J, Yang J, Lang J, Cao J, Liu F, et al. Size-controlled fabrication of ZnO micro/nanorod arrays and their photocatalytic performance. *Materials Chemistry and Physics*. 2013;**141**:929-935. DOI: 10.1016/j.matchemphys.2013.06.028
- [25] Yin M, Liu M, Liu S. Diameter regulated ZnO nanorod synthesis and its application in gas sensor optimization. *Journal of Alloys and Compounds*. 2014;**586**:436-440. DOI: 10.1016/j.jallcom.2013.10.081
- [26] Chen T-Y, Chen H-I, Hsu C-S, Huang C-C, Wu J-S, Chou P-C, et al. Characteristics of ZnO nanorods-based ammonia gas sensors with a cross-linked configuration. *Sensors and Actuators B: Chemical*. 2015;**221**:491-498. DOI: 10.1016/j.snb.2015.06.122
- [27] Hosseini ZS, Zad AI, Mortezaali A. Room temperature H<sub>2</sub>S gas sensor based on rather aligned ZnO nanorods with flower-like structures. *Sensors and Actuators B: Chemical*. 2015;**207**:865-871. DOI: 10.1016/j.snb.2014.10.085
- [28] Hu P, Han N, Zhang X, Yao M, Cao Y, Zuo A, et al. Fabrication of ZnO nanorod-assembled multishelled hollow spheres and enhanced performance

in gas sensor. *Journal of Materials Chemistry*. 2011;**21**(37):14277. DOI: 10.1039/c1jm11919b

[29] Zhang H, Wu J, Zhai C, Du N, Ma X, Yang D. From ZnO nanorods to 3D hollow microhemispheres: Solvothermal synthesis, photoluminescence and gas sensor properties. *Nanotechnology*. 2007;**18**(45):455604. DOI: 10.1088/0957-4484/18/45/455604

[30] Lee WC, Fang Y, Turner JFC, Bedi JS, Perry CC, He H, et al. An enhanced gas ionization sensor from Y-doped vertically aligned conductive ZnO nanorods. *Sensors and Actuators B: Chemical*. 2016;**237**:724-732. DOI: 10.1016/j.snb.2016.06.146

[31] Zhang GH, Deng XY, Wang PY, Wang XL, Chen Y, Ma HL, et al. Morphology controlled syntheses of Cr doped ZnO single-crystal nanorods for acetone gas sensor. *Materials Letters*. 2016;**165**:83-86. DOI: 10.1016/j.matlet.2015.11.112

[32] Rai P, Jeon SH, Lee CH, Lee JH, Yu YT. Functionalization of ZnO nanorods by CuO nanospikes for gas sensor applications. *RSC Advances*. 2014;**4**(45):23604-23609. DOI: 10.1039/c4ra00078a

[33] Hieu NM, Kim H, Kim C, Hong S-K, Kim D. A hydrogen sulfide gas sensor based on Pd-decorated ZnO nanorods. *Journal of Nanoscience and Nanotechnology*. 2016;**16**(10):10351-10355. DOI: 10.1166/jnn.2016.13158

[34] Sun GJ, Lee JK, Choi S, Lee WI, Kim HW, Lee C. Selective oxidizing gas sensing and dominant sensing mechanism of N-CaO-decorated N-ZnO nanorod sensors. *ACS Applied Materials and Interfaces*. 2017;**9**(11):9975-9985. DOI: 10.1021/acsami.6b15995

[35] Wu X, Xiong S, Mao Z, Hu S, Long X. A designed ZnO@Zif-8 core-shell nanorod film as a gas sensor

with excellent selectivity for H<sub>2</sub> over CO. *Chemistry-A European Journal*. 2017;**23**(33):7969-7975. DOI: 10.1002/chem.201700320

[36] Zhang D, Sun Y, Zhang Y. Fabrication and characterization of layer-by-layer nano self-assembled ZnO nanorods/carbon nanotube film sensor for ethanol gas sensing application at room temperature. *Journal of Materials Science: Materials in Electronics*. 2015;**26**(10):7445-7451. DOI: 10.1007/s10854-015-3378-4

[37] Si S, Li C, Wang X, Peng Q, Li Y. Fe<sub>2</sub>O<sub>3</sub>/ZnO core-shell nanorods for gas sensors. *Sensors and Actuators B: Chemical*. 2006;**119**(1):52-56. DOI: 10.1016/j.snb.2005.11.050

[38] Jin C, Park S, Kim H, Lee C. Ultrasensitive multiple networked Ga<sub>2</sub>O<sub>3</sub>-core/ZnO-shell nanorod gas sensors. *Sensors and Actuators B: Chemical*. 2012;**161**(1):223-228. DOI: 10.1016/j.snb.2011.10.023

[39] Park S, Kim H, Jin C, Lee C. Enhanced gas sensing properties of multiple networked In<sub>2</sub>O<sub>3</sub>-core/ZnO-shell nanorod sensors. *Journal of Nanoscience and Nanotechnology*. 2013;**13**(5):3427-3432. DOI: 10.1166/jnn.2013.7231

[40] Yi J, Lee JM, Park WI. Vertically aligned ZnO nanorods and graphene hybrid architectures for high-sensitive flexible gas sensors. *Sensors and Actuators B: Chemical*. 2011;**155**(1):264-269. DOI: 10.1016/j.snb.2010.12.033